A Comparison of the Performance of Limiters for Runge-Kutta Discontinuous Galerkin Methods

Hongqiang Zhu[1], Yue Cheng[2,4] and Jianxian Qiu[3,*]

[1] *School of Natural Science, Nanjing University of Posts and Telecommunications, Nanjing, Jiangsu 210023, China*
[2] *Department of Mathematics, Nanjing University, Nanjing, Jiangsu 210093, China*
[3] *School of Mathematical Sciences, Xiamen University, Xiamen, Fujian 361005, China*
[4] *Baidu, Inc. Baidu Campus, No. 10, Shangdi 10th Street, Haidian District, Beijing 100085, China*

Abstract. Discontinuities usually appear in solutions of nonlinear conservation laws even though the initial condition is smooth, which leads to great difficulty in computing these solutions numerically. The Runge-Kutta discontinuous Galerkin (RKDG) methods are efficient methods for solving nonlinear conservation laws, which are high-order accurate and highly parallelizable, and can be easily used to handle complicated geometries and boundary conditions. An important component of RKDG methods for solving nonlinear conservation laws with strong discontinuities in the solution is a nonlinear limiter, which is applied to detect discontinuities and control spurious oscillations near such discontinuities. Many such limiters have been used in the literature on RKDG methods. A limiter contains two parts, first to identify the "troubled cells", namely, those cells which might need the limiting procedure, then to replace the solution polynomials in those troubled cells by reconstructed polynomials which maintain the original cell averages (conservation). [SIAM J. Sci. Comput., 26 (2005), pp. 995–1013.] focused on discussing the first part of limiters. In this paper, focused on the second part, we will systematically investigate and compare a few different reconstruction strategies with an objective of obtaining the most efficient and reliable reconstruction strategy. This work can help with the choosing of right limiters so one can resolve sharper discontinuities, get better numerical solutions and save the computational cost.

*Corresponding author.
URL: http://ccam.xmu.edu.cn/teacher/jxqiu
Email: zhuhq@njupt.edu.cn (H. Zhu), chengyue127@gmail.com (Y. Cheng), jxqiu@xmu.edu.cn (J. Qiu)

1 Introduction

The Runge-Kutta discontinuous Galerkin (RKDG) methods for solving hyperbolic conservation laws are high-order accurate and highly parallelizable methods which can easily handle complicated geometries and boundary conditions. These methods have made their way into the main stream of computational fluid dynamics and other areas of applications. The first DG method was introduced in 1973 by Reed and Hill [15] for the neutron transport problem. A major development of this method was carried out by Cockburn et al. in a series of papers [3–7], in which a framework to solve nonlinear time dependent hyperbolic conservation laws was established. They adopted explicit, nonlinearly stable high order Runge-Kutta time discretizations [18], DG space discretizations with exact or approximate Riemann solvers as interface fluxes and TVB (total variation bounded) nonlinear limiter [17] to achieve nonoscillatory properties, and the method was termed as RKDG method. We will briefly review this method in Section 2. Detailed description of the method as well as its implementation can be found in the review paper [8].

Solutions of nonlinear hyperbolic conservation laws usually have discontinuities even though the initial conditions are smooth, which leads to great difficulty in computing these solutions numerically. An important component of RKDG methods for solving conservation laws with strong shocks in the solution is a nonlinear limiter, which is applied to detect discontinuities and control spurious oscillations near such discontinuities. Many such limiters have been used in the RKDG methods. Cockburn et al. developed the minmod-type TVB limiter [3–7], which is a slope limiter using a technique borrowed from the finite volume methodology. Biswas et al. proposed a moment limiter [1] which is specifically designed for DG methods and works on the moments of the numerical solution. This moment limiter was later improved by Burbeau et al. [2] and improved further by Krivodonova [10]. There are also many limiters developed in the finite volume and finite difference literature, such as various flux limiters [21], monotonicity-preserving (MP) limiters [20] and modified MP limiters [16].

Although there are many limiters that we can use in the RKDG methods, none of them is reported to be obviously better than the others for various problems. Numerical experiments in the literature tell that different limiters usually behave differently for the same problem and the same limiter may behave differently for different problems. There is no guideline for people to choose a right limiter for a certain problem. So a systematic study of limiters is necessary.

Qiu and Shu [14] adopted a new framework to devise a limiter for the RKDG methods. They divided a limiter into two separate parts. The first part is a "troubled-cell indicator", which is a discontinuity detection strategy which detects the cells that are believed to contain a discontinuity and need the limiting procedure. The second part is a solution reconstruction method which is applied only on the detected cells. The troubled-cell indicators can come from any limiters or shock detecting techniques. Focused on the first part of limiters, Qiu and Shu [13] presented an overview of the troubled-cell indicators and made a comparison of their performance in conjunction with a high-order

WENO (weighted essentially nonoscillatory) solution reconstruction method. In this paper, focused on the second part, we will systematically investigate and compare a few different reconstruction strategies with an objective of obtaining the most efficient and reliable reconstruction strategy. This work can help with the choosing of right limiters so one can resolve sharper discontinuities, get better numerical solutions and save the computational cost.

The outline of the remainder of the paper is as follows. In Section 2 we briefly review the RKDG methods in one dimension. Section 3 reviews the limiters used in this paper. Numerical comparisons and computational results on a variety of test cases are presented in Section 4 with conclusions following in Section 5.

2   Review of RKDG method

We consider the one-dimensional scalar conservation law

$$\begin{cases} u_t + f(u)_x = 0, \\ u(x,0) = u_0(x). \end{cases} \tag{2.1}$$

We divide the computational domain $[0,L]$ into N cells with boundary points

$$0 = x_{\frac{1}{2}} < x_{\frac{3}{2}} < \cdots < x_{N+\frac{1}{2}} = L.$$

Denote the center of cell $I_i = [x_{i-\frac{1}{2}}, x_{i+\frac{1}{2}}]$ by x_i, and the length of cell I_i by Δx_i. The solution as well as the test function space is given by $V_h^k = \{p : p|_{I_i} \in P_k(I_i)\}$, where $P_k(I_i)$ is the space of polynomials of degree at most k on cell I_i. We adopt the Legendre polynomials

$$W_0(x) = 1, \quad W_l(x) = \frac{1}{2^l l!} \frac{d^l (x^2 - 1)^l}{dx^l}, \quad l = 1, \cdots, k, \tag{2.2}$$

as the local basis functions. However, we emphasize that the procedure described below does not depend on the specific basis chosen for the polynomials and works also in multiple dimensions. The Legendre polynomials are L_2-orthogonal, namely,

$$\int_{-1}^{1} W_l(x) W_{l'}(x) dx = \begin{cases} \dfrac{2}{2l+1}, & \text{if } l = l', \\ 0, & \text{otherwise.} \end{cases}$$

And now we can express our approximate solution u^h as follows:

$$u^h(x,t) = \sum_{l=0}^{k} u_i^{(l)}(t) v_l^{(i)}(x) \quad \text{for } x \in I_i, \tag{2.3}$$

where

$$v_l^{(i)}(x) = W_l(2(x - x_i)/\Delta x_i),$$

and $u_i^{(l)}(t)$ $(l=0,\cdots,k)$ are the degrees of freedom. We will omit the argument t and denote them as $u_i^{(l)}$ in this paper.

In order to determine the approximate solution, we multiply (2.1) by test functions $v_l^{(i)}(x)$ $(l=0,\cdots,k)$, integrate over cell I_i, integrate by parts, and we are able to evolve the degrees of freedom $u_i^{(l)}$:

$$\frac{\Delta x_i}{2l+1}\frac{d}{dt}u_i^{(l)}-\int_{I_i}f(u^h(x,t))\frac{dv_l^{(i)}(x)}{dx}dx+\hat{f}(u_{i+\frac{1}{2}}^-,u_{i+\frac{1}{2}}^+)$$
$$-(-1)^l\hat{f}(u_{i-\frac{1}{2}}^-,u_{i-\frac{1}{2}}^+)=0,\quad l=0,\cdots,k,\tag{2.4}$$

where $u_{i+1/2}^{\pm}=u^h(x_{i+1/2}^{\pm},t)$ are the left and right limits of the discontinuous solution u^h at the cell interface $x_{i+1/2}$, and $\hat{f}(u^-,u^+)$ is a consistent and monotone (nondecreasing in the first argument and nonincreasing in the second argument) flux for the scalar case and an exact or approximate Riemann solver for the system case. The semidiscrete scheme (2.4) is an ODE system. One discretizes it using the total variation diminishing (TVD) Runge-Kutta time discretization introduced in [18], which completes the definition of RKDG method. In this paper for $k=1$, we use the second order Runge-Kutta time stepping

$$\phi^{(1)}=\phi^n+\Delta tL(\phi^n),\tag{2.5a}$$
$$\phi^{n+1}=\frac{1}{2}\phi^n+\frac{1}{2}\phi^{(1)}+\frac{1}{2}\Delta tL(\phi^{(1)}),\tag{2.5b}$$

if the ODE system is denoted by $\phi_t=L(\phi)$. For $k=2$, we use the following third order version

$$\phi^{(1)}=\phi^n+\Delta tL(\phi^n),\tag{2.6a}$$
$$\phi^{(2)}=\frac{3}{4}\phi^n+\frac{1}{4}\phi^{(1)}+\frac{1}{4}\Delta tL(\phi^{(1)}),\tag{2.6b}$$
$$\phi^{n+1}=\frac{1}{3}\phi^n+\frac{2}{3}\phi^{(2)}+\frac{2}{3}\Delta tL(\phi^{(2)}).\tag{2.6c}$$

3 Description of limiters

In this section, we describe a few commonly used limiters which are chosen for our numerical comparisons.

1. Minmod-based TVB limiter (TVB limiter) [5]. Denote

$$u_{i+\frac{1}{2}}^-=u_i^{(0)}+\tilde{u}_i,\qquad u_{i-\frac{1}{2}}^+=u_i^{(0)}-\tilde{\tilde{u}}_i.\tag{3.1}$$

From (2.3) we can derive

$$\tilde{u}_i=\sum_{l=1}^k u_i^{(l)}v_l^{(i)}(x_{i+\frac{1}{2}}),\qquad \tilde{\tilde{u}}_i=-\sum_{l=1}^k u_i^{(l)}v_l^{(i)}(x_{i-\frac{1}{2}}).\tag{3.2}$$

They are modified by the TVB-modified minmod function

$$\tilde{u}_i^{(mod)} = \tilde{m}(\tilde{u}_i, u_{i+1}^{(0)} - u_i^{(0)}, u_i^{(0)} - u_{i-1}^{(0)}), \tag{3.3a}$$

$$\tilde{\tilde{u}}_i^{(mod)} = \tilde{m}(\tilde{\tilde{u}}_i, u_{i+1}^{(0)} - u_i^{(0)}, u_i^{(0)} - u_{i-1}^{(0)}), \tag{3.3b}$$

where $\tilde{m}$ is given by

$$\tilde{m}(a_1, a_2, \cdots, a_n) = \begin{cases} a_1, & \text{if } |a_1| \leq Mh^2, \\ m(a_1, a_2, \cdots, a_n), & \text{otherwise,} \end{cases} \tag{3.4}$$

and the minmod function m is given by

$$m(a_1, a_2, \cdots, a_n) = \begin{cases} s \cdot \min_{1 \leq j \leq n} |a_j|, & \text{if } \mathrm{sign}(a_1) = \mathrm{sign}(a_2) = \cdots = \mathrm{sign}(a_n) = s, \\ 0, & \text{otherwise.} \end{cases} \tag{3.5}$$

The parameter $M > 0$ is a constant.

Unfortunately, the TVB limiter constant M is dependent on the problem. There is no automatic switching which works well for various situations. As it was pointed out in [4], the resolution of solution is dependent on the choice of the constant M; and sometimes, the case of $k = 1$ may give better resolution to shocks or contact discontinuities than the case of $k = 2$ if an inappropriate M is used. Tuning M requires much experimental research. But once we get the appropriate M, the TVB limiter will make the solution much better. In this paper, M is chosen based on our numerical trials and experience and the corresponding limiter is denoted by TVB-2.

2. Moment limiter of Biswas, Devine, and Flaherty (BDF limiter) [1]. The moments are modified as follows:

$$u_i^{(l),mod} = \frac{1}{2l-1} m\left((2l-1)u_i^{(l)}, u_{i+1}^{(l-1)} - u_i^{(l-1)}, u_i^{(l-1)} - u_{i-1}^{(l-1)}\right), \quad 1 \leq l \leq k, \tag{3.6}$$

where m is again the minmod function. This limiter is applied adaptively. First, the highest-order moment $u^{(k)}$ is limited. Then the limiter is applied successively to lower-order moments when the next higher-order moment has been changed by the limiting.

3. A modification of the moment limiter by Burbeau, Sagaut, and Bruneau (BSB limiter) [2]. We define

$$u_i^{(l),m} = \frac{1}{2l-1} m\left((2l-1)u_i^{(l)}, u_{i+1}^{(l-1)} - u_i^{(l-1)}, u_i^{(l-1)} - u_{i-1}^{(l-1)}\right), \quad 1 \leq l \leq k. \tag{3.7}$$

If $u_i^{(l),m} \neq u_i^{(l)}$, the moment $u_i^{(l)}$ is replaced with

$$u_i^{(l),mod} = \mathrm{maxmod}\left(u_i^{(l),m}, u_i^{(l),\max}\right), \tag{3.8}$$

where

$$\text{maxmod}(a_1,a_2,\cdots,a_n)=\begin{cases} s\cdot\max_{1\le j\le n}|a_j|, & \text{if } \text{sign}(a_1)=\cdots=\text{sign}(a_n)=s,\\ 0, & \text{otherwise,}\end{cases} \tag{3.9a}$$

$$u_i^{(l),\max}=\frac{1}{2l-1}m\Big((2l-1)u_i^{(l)},u_{i+\frac{1}{2}}^{(l-1)+}-u_i^{(l-1)},u_i^{(l-1)}-u_{i-\frac{1}{2}}^{(l-1)-}\Big), \tag{3.9b}$$

$$u_{i+\frac{1}{2}}^{(l-1)+}=u_{i+1}^{(l-1)}-(2l-1)u_{i+1}^{(l)},\quad u_{i-\frac{1}{2}}^{(l-1)-}=u_{i-1}^{(l-1)}+(2l-1)u_{i-1}^{(l)}. \tag{3.9c}$$

This limiting procedure is applied in the same adaptive way as BDF limiter.

4. A monotonicity-preserving limiter (MP limiter) [20]. Define

$$\text{median}(x,y,z)=x+m(y-x,z-x), \tag{3.10}$$

where m is the minmod function. We modify the point value

$$u_{i+\frac{1}{2}}^{-,mod}=\text{median}\big(u_{i+\frac{1}{2}}^-,u_{i+\frac{1}{2}}^{\min},u_{i+\frac{1}{2}}^{\max}\big), \tag{3.11}$$

where

$$u_{i+\frac{1}{2}}^{\min}=\max\Big[\min(u_i^{(0)},u_{i+1}^{(0)},u_{i+\frac{1}{2}}^{MD}),\min(u_i^{(0)},u_{i+\frac{1}{2}}^{UL},u_{i+\frac{1}{2}}^{LC})\Big], \tag{3.12a}$$

$$u_{i+\frac{1}{2}}^{\max}=\min\Big[\max(u_i^{(0)},u_{i+1}^{(0)},u_{i+\frac{1}{2}}^{MD}),\max(u_i^{(0)},u_{i+\frac{1}{2}}^{UL},u_{i+\frac{1}{2}}^{LC})\Big], \tag{3.12b}$$

and

$$d_i=u_{i+1}^{(0)}-2u_i^{(0)}+u_{i-1}^{(0)}, \tag{3.13a}$$

$$d_{i+\frac{1}{2}}^{M4X}=m(4d_i-d_{i+1},4d_{i+1}-d_i,d_i,d_{i+1},d_{i-1},d_{i+2}), \tag{3.13b}$$

$$u_{i+\frac{1}{2}}^{MD}=\frac{1}{2}\Big(u_i^{(0)}+u_{i+1}^{(0)}-d_{i+\frac{1}{2}}^{M4X}\Big),\quad u_{i+\frac{1}{2}}^{UL}=u_i^{(0)}+\alpha\Big(u_i^{(0)}-u_{i-1}^{(0)}\Big), \tag{3.13c}$$

$$u_{i+\frac{1}{2}}^{LC}=u_i^{(0)}+\frac{1}{2}\Big(u_i^{(0)}-u_{i-1}^{(0)}\Big)+\frac{\beta}{3}d_{i-\frac{1}{2}}^{M4X}. \tag{3.13d}$$

The point value $u_{i-\frac{1}{2}}^+$ is modified in a similar (symmetric) way. We take the parameters $\alpha=2$ and $\beta=4$ in the numerical tests in the next section, as suggested in [20].

5. A modified MP limiter (MMP limiter) [16]. The moments are limited to

$$u_i^{(l),mod}=\phi_i u_i^{(l)},\quad 1\le l\le k, \tag{3.14}$$

where

$$\phi_i=\min(1,|u_i^{(0)}|/\Delta_{\min}u_i),\quad \Delta_{\min}u_i=u_i^{(0)}-\min_{x\in I_i}u^h(x,t). \tag{3.15}$$

This limiter relaxes the constraint of preserving monotonicity while enforcing weaker constraints and is a sign-preserving limiter.

6. A shock-detection technique by Krivodonova et al. (KXRCF shock-detector) [11]. Partition the boundary of a cell I_i into two portions ∂I_i^- and ∂I_i^+, where the flow is into ($\vec{v} \cdot \vec{n} < 0$, $\vec{n}$ is the normal vector to ∂I_i) and out of ($\vec{v} \cdot \vec{n} > 0$) I_i, respectively. The cell I_i is believed to contain a discontinuity if

$$\frac{\left| \int_{\partial I_i^-} (u^h|_{I_i} - u^h|_{I_{n_i}}) ds \right|}{\Delta x_i^{\frac{k+1}{2}} |\partial I_i^-| \, \||u^h|_{I_i}\|} > 1. \tag{3.16}$$

Here I_{n_i} is the neighbor of I_i on the side of ∂I_i^- and the norm is based on an element average in one dimension.

This KXRCF shock-detector functions as the first part of the limiter, that is a troubled-cell indicator. It is one of the three recommended troubled-cell indicators in the comparison of different troubled-cell indicators carried out by Qiu and Shu [13]. It is also one of the best troubled-cell indicators for the h- and r-adaptive RKDG methods presented in [25]. The good performance of this shock-detector motivates us to use it to design new limiters. In this paper, we add this shock-detector to the original limiters described above to form new limiters and compare their performance. Each new limiter works in the following way. It first uses KXRCF shock-detector to identify troubled-cells, and then applies the original limiter only in these troubled-cells. We also combine this shock-detector with the WENO solution reconstruction method introduced in [14] and a simple WENO solution reconstruction method recently introduced in [24] (which are both described below), and the resulting limiters are denoted by WENO limiter and SWENO limiter, respectively. For the sake of convenience, all the limiters in this paper that involve KXRCF shock-detector are called by KXRCF-type limiters. If a KXRCF-type limiter is added to an original limiter, it is denoted by adding "(K)" after the name of the original limiter, for example TVB-2(K) limiter.

7. WENO solution reconstruction method [14]. From (2.3) we can derive

$$u_i^{(l)} = \frac{2l+1}{\Delta x_i} \int_{I_i} u_h(x,t) v_l^{(i)}(x) dx, \quad l = 0, \cdots, k. \tag{3.17}$$

If we use numerical quadratures to compute the integrations in (3.17), to reconstruct cell I_i's degrees of freedom $u_i^{(l)}$ ($l = 1, \cdots, k$), all we have to do is to reconstruct the point values of u^h at the quadrature points. As is indicated in [14], the following particular quadrature points are used:

- $k = 1$: two-point Gauss quadrature points $x_{i-\frac{\sqrt{3}}{6}}$ and $x_{i+\frac{\sqrt{3}}{6}}$;

- $k = 2$: four-point Gauss-Lobatto quadrature points $x_{i-\frac{1}{2}}$, $x_{i-\frac{\sqrt{5}}{10}}$, $x_{i+\frac{\sqrt{5}}{10}}$ and $x_{i+\frac{1}{2}}$.

Let us now reconstruct the point value at some quadrature point x_G. For $j = 0, \cdots, k$, we have a k-th degree polynomial reconstruction $p_j(x)$ such that

$$\frac{1}{\Delta x_{i+j-l}} \int_{I_{i+j-l}} p_j(x) dx = u_{i+j-l}^{(0)}, \quad l = 0, \cdots, k. \tag{3.18}$$

We also have a $2k$-th degree polynomial reconstruction $Q(x)$ such that

$$\frac{1}{\Delta x_{i+l}} \int_{I_{i+l}} Q(x)dx = u_{i+l}^{(0)}, \quad l=-k,\cdots,k. \tag{3.19}$$

Find the so called linear weights $\gamma_0,\cdots,\gamma_k$, which satisfy

$$Q(x_G) = \sum_{j=0}^{k} \gamma_j p_j(x_G). \tag{3.20}$$

Then we compute the smoothness indicators

$$\beta_j = \sum_{l=1}^{k} \int_{I_i} \Delta x_i^{2l-1} \left(\frac{\partial^l}{\partial x^l} p_j(x)\right)^2 dx, \quad j=0,\cdots,k, \tag{3.21}$$

and the nonlinear weights $\omega_0,\cdots,\omega_k$,

$$\omega_j = \frac{\bar{\omega}_j}{\sum_j \bar{\omega}_j}, \quad \bar{\omega}_j = \frac{\gamma_j}{(\varepsilon+\beta_j)^2}, \quad j=0,\cdots,k. \tag{3.22}$$

ε is a small number to avoid the denominator becoming zero. We use $\varepsilon = 10^{-6}$ in all computations in this paper. The final WENO approximation is then given by

$$u^{\text{WENO}}(x_G) = \sum_{j=0}^{k} \omega_j p_j(x_G). \tag{3.23}$$

8. A simple WENO solution reconstruction method [24]. Assume that we need to reconstruct the solution on cell I_i. Denote the DG solution polynomial of u on cells I_{i-1}, I_i, I_{i+1} as $p_0(x)$, $p_1(x)$, $p_2(x)$, respectively. Denote

$$\tilde{p}_0(x) = p_0(x) - \bar{\bar{p}}_0 + \bar{\bar{p}}_1, \quad \tilde{p}_2(x) = p_2(x) - \bar{\bar{p}}_2 + \bar{\bar{p}}_1, \tag{3.24}$$

where

$$\bar{\bar{p}}_j = \frac{1}{\Delta x_i} \int_{I_i} p_j(x)dx, \quad j=0,1,2. $$

We first compute the smoothness indicators

$$\beta_j = \sum_{l=1}^{k} \int_{I_i} \Delta x_i^{2l-1} \left(\frac{\partial^l}{\partial x^l} p_j(x)\right)^2 dx, \quad j=0,1,2. \tag{3.25}$$

For any linear weights γ_0, γ_1, γ_2, we then compute the nonlinear weights ω_0, ω_1, ω_2

$$\omega_j = \frac{\bar{\omega}_j}{\sum_j \bar{\omega}_j}, \quad \bar{\omega}_j = \frac{\gamma_j}{(\varepsilon+\beta_j)^2}, \quad j=0,1,2. \tag{3.26}$$

Finally, the final WENO reconstruction polynomial is given by

$$p_1^{\text{SWENO}}(x) = \omega_0 \tilde{p}_0(x) + \omega_1 p_1(x) + \omega_2 \tilde{p}_2(x). \tag{3.27}$$

We take $\varepsilon = 10^{-6}$, $\gamma_0 = 0.001$, $\gamma_1 = 0.998$, $\gamma_2 = 0.001$ in our numerical tests as in [24].

Remark 3.1. For the case of hyperbolic systems, all the limiting procedures in this section are performed in local characteristic directions. For details we refer to [4, 9]. The two-dimensional case is not covered because of space limitation. We refer to the corresponding original paper of each limiter.

4 Numerical tests and comparisons

In this section we provide a series of numerical examples to test and compare the limiters. The limiters are performed after each inner stage in the Runge-Kutta time stepping. A positivity-preserving technique [22] is used in all the test problems in order to avoid negative density or negative pressure during the time evolution. We will focus on the percentage of limited cells and the control of spurious oscillations in the comparison according to the functions of limiters. Also, we will only plot the uniform-mesh results obtained with a particular choice of cell number N to save space, and only plot the discontinuous regions (which we are interested in) in the solution figures for a better view of details.

We use the one-dimensional Euler equations of gas dynamics with different initial data as our one-dimensional test problems. The Euler equations are

$$\left[\begin{array}{c} \rho \\ \rho v \\ E \end{array}\right]_t + \left[\begin{array}{c} \rho v \\ \rho v^2 + p \\ v(E+p) \end{array}\right]_x = 0. \tag{4.1}$$

Here ρ is the density, v is the velocity, E is the total energy, p is the pressure, related to the total energy by $E = p/(\gamma-1) + \rho v^2/2$ with $\gamma = 1.4$.

Example 4.1. Single contact discontinuity. The initial condition is

$$(\rho, v, p) = \left\{ \begin{array}{ll} (\eta_\rho, 1, 1), & \text{if } x \leq 0, \\ (1, 1, 1), & \text{otherwise.} \end{array} \right.$$

We choose $\eta_\rho = 10^n$ ($n = 1, \cdots, 6$) in the numerical running but only the results for $\eta_\rho = 10^6$ are shown because the results for other choices of η_ρ are similar. The computational domain is $[-5,5]$. In TVB-2 limiter, the parameter $M = 100$. We plot the density solutions on $[2.5,3.5]$ at $T = 3$ in Figs. 1 and 2. In these figures the solid line is the reference exact solution and each "□" or "+" represents average density of a cell.

In Figs. 1 and 2 we can see that for the original limiters, contact discontinuities are well resolved with TVB-2, BDF, BSB and MP limiters while oscillations appear with MMP limiter for both $k = 1$ and $k = 2$ cases. For the KXRCF-type limiters, there are oscillations near the discontinuity in all the cases of $k = 1$. For $k = 2$ all the solutions are well resolved except that slight oscillations are observed with MMP(K) limiter. Compared to the original limiters, adding KXRCF shock-detector causes slight oscillations for TVB, BDF, BSB and MP limiters when $k = 1$.
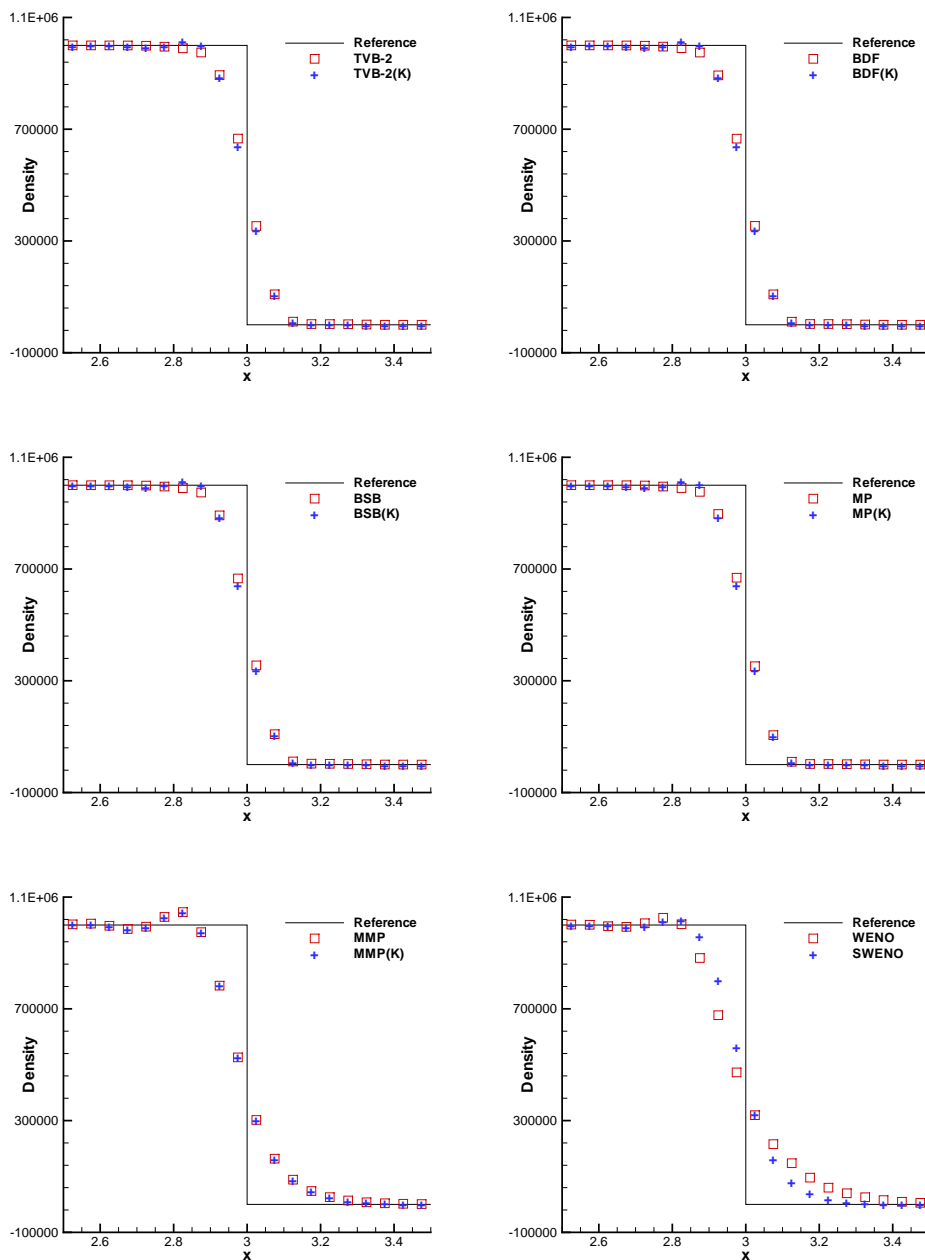
Figure 1: Single contact discontinuity, density solutions, $\eta_\rho = 10^6$, $N = 200$, $k = 1$.

In order to compare the limiting efficiency, we mark every limited cell at each time step and compute the average and maximum percentage of limited cells through all time steps. These data are tabulated in Table 1, in which "Ave" and "Max" denote the average and maximum percentage of limited cells, respectively, and those data derived with
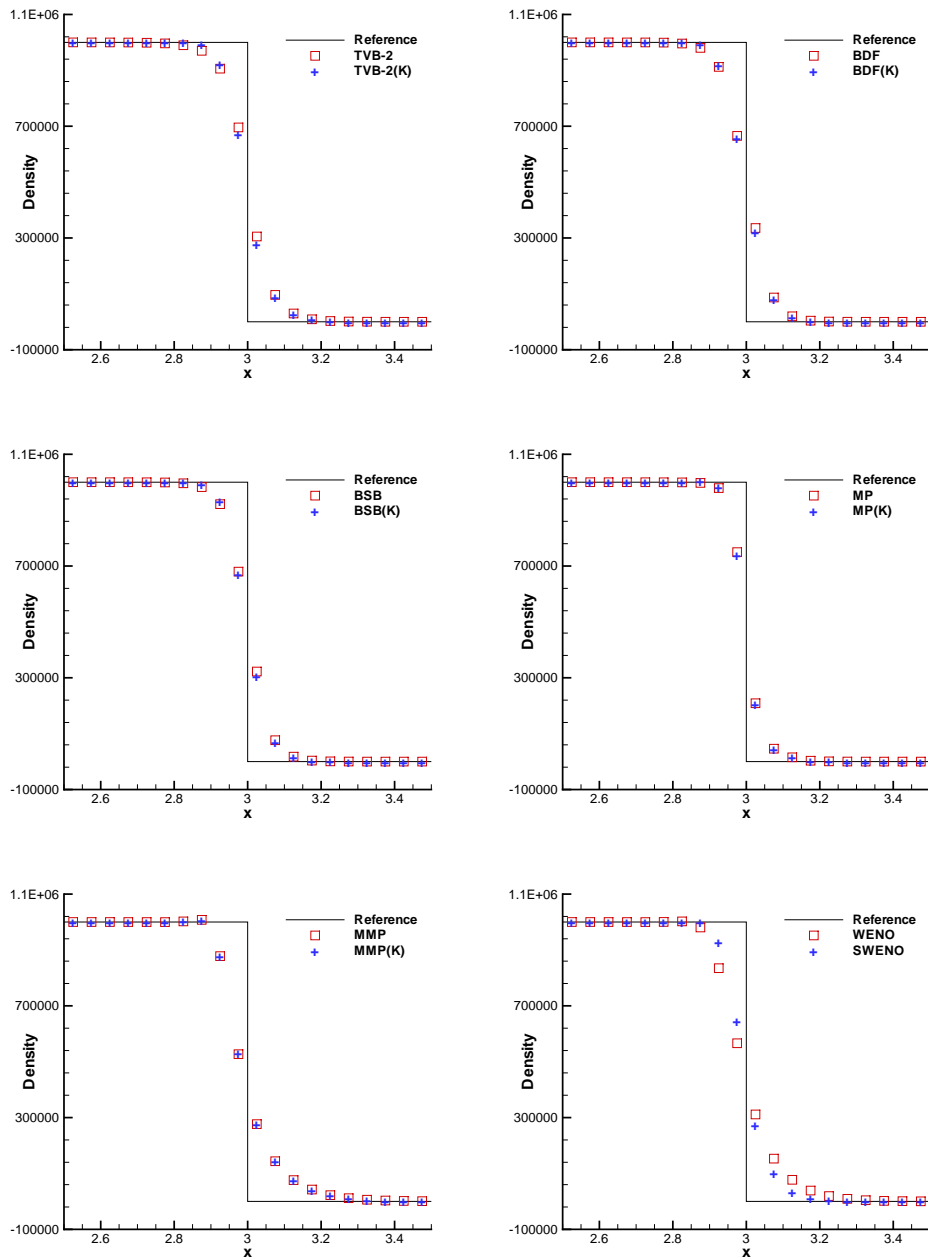
Figure 2: Single contact discontinuity, density solutions, $\eta_\rho = 10^6$, $N = 200$, $k = 2$.

KXRCF-type limiters are marked with "(K)". This table demonstrates the different behaviors of different limiters for the same problem. In this test problem BDF, BSB and MP limiters do much more limiting than the other original limiters. For KXRCF-type limiters, all of them do a low amount of limiting, no matter how much limiting their cor-

Table 1: Single contact discontinuity, average and maximum percentage of limited cells, $N=200$.

Limiter	$k=1$				$k=2$			
	Ave	Max	Ave(K)	Max(K)	Ave	Max	Ave(K)	Max(K)
TVB-2	3.53	5.50	1.98	4.00	5.42	10.00	0.77	7.50
BDF	16.36	27.00	4.57	7.00	43.06	87.50	4.73	7.00
BSB	32.68	65.50	4.20	6.50	63.16	86.00	4.74	7.00
MP	69.65	94.00	5.37	8.00	67.16	85.50	3.03	6.50
MMP	9.25	10.00	7.58	9.50	9.04	10.00	6.37	9.50
WENO	–	–	9.32	12.50	–	–	7.91	9.50
SWENO	–	–	10.80	13.50	–	–	6.21	8.00

responding original limiters do. For this problem, using KXRCF shock-detector to locate discontinuous regions before limiting reduces the solution reconstruction work to a low amount.

Example 4.2. Single shock. The initial condition is

$$(\rho, v, p) = \begin{cases} (1,0,1), & \text{if } x \le 0, \\ \left(\dfrac{1+6\eta_p}{\eta_p+6}, \dfrac{1-\eta_p}{\sqrt{1.2\eta_p+0.2}}, \eta_p \right), & \text{otherwise.} \end{cases}$$

We choose $\eta_p = 10^n$ $(n=2,\cdots,5)$ in the numerical running but only show the results for $\eta_p = 10^5$. The computational domain is $[-50,50]$ and the parameter $M=20$ in TVB-2 limiter. We solve this problem till $T=0.1$.

We plot the density solutions on $[-37,-32]$ in Figs. 3 and 4. We observe slight oscillations for BSB(K) limiter and obvious oscillations for MMP and MMP(K) limiters in both $k=1$ and $k=2$ cases. The shocks are smeared more with WENO limiter though it is oscillatory free, and SWENO limiter smears the most in this test problem.

Table 2 gives average and maximum percentage of limited cells. We again see that BDF, BSB and MP limiters do much more limiting while all the other limiters do a comparable low amount of limiting.

Table 2: Single shock, average and maximum percentage of limited cells, $N=1000$.

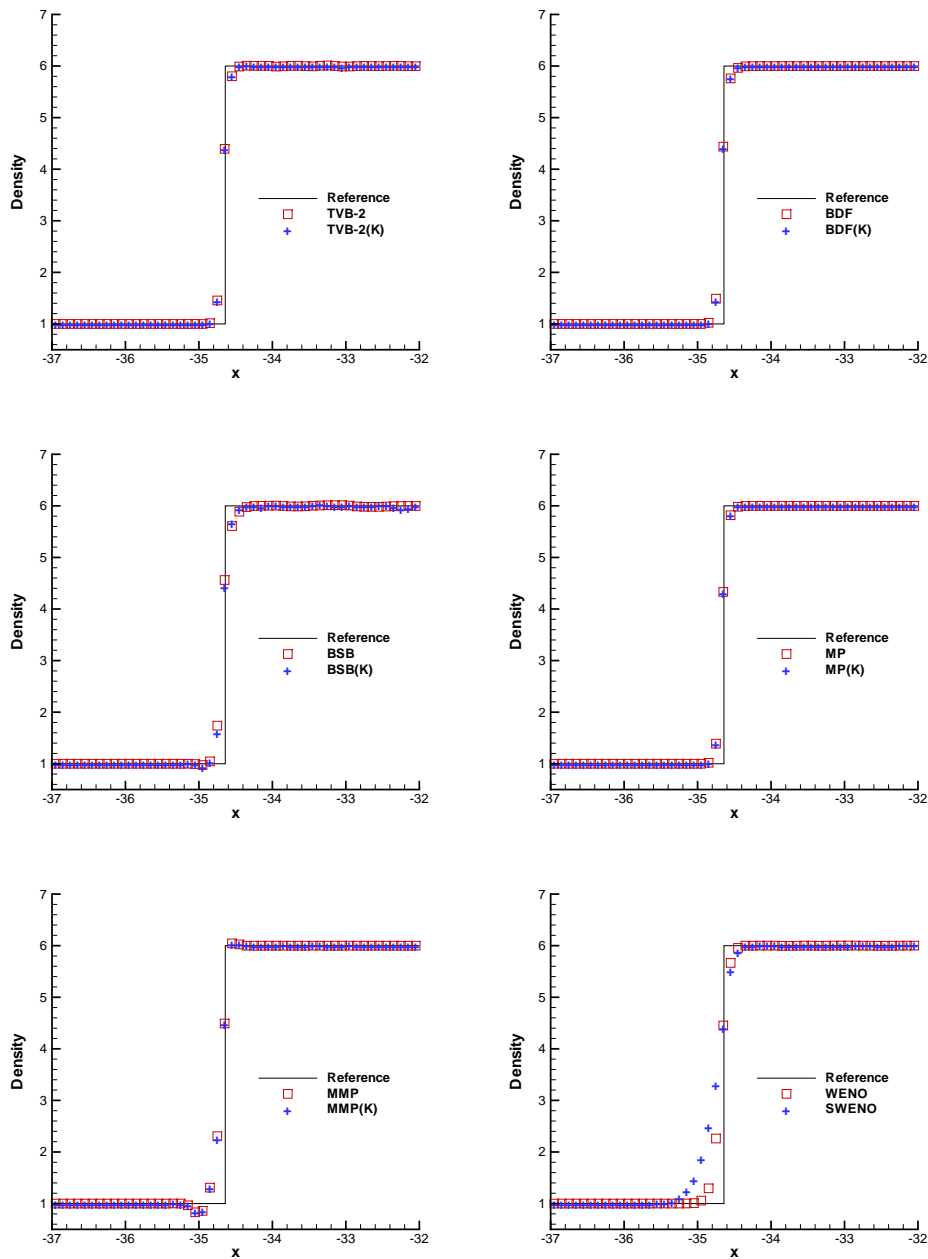| Limiter	$k=1$				$k=2$			
	Ave	Max	Ave(K)	Max(K)	Ave	Max	Ave(K)	Max(K)
TVB-2	0.36	0.50	0.34	0.50	1.09	1.30	1.08	1.30
BDF	8.16	15.60	0.43	0.50	11.38	21.10	0.69	0.80
BSB	11.19	21.60	0.48	0.70	12.62	23.50	0.72	1.00
MP	9.58	15.00	0.49	0.60	10.29	19.30	0.90	1.10
MMP	0.45	0.50	0.44	0.50	0.84	0.90	0.84	0.90
WENO	–	–	0.74	0.90	–	–	0.70	0.80
SWENO	–	–	1.24	1.50	–	–	1.23	1.60

Figure 3: Single shock, density solutions, $\eta_p = 10^5$, $N = 1000$, $k = 1$.

Example 4.3. Lax problem [12]. The initial condition is

$$(\rho, v, p) = \begin{cases} (0.445, 0.698, 3.528), & \text{if } x \le 0, \\ (0.5, 0, 0.571), & \text{if } x > 0. \end{cases}$$
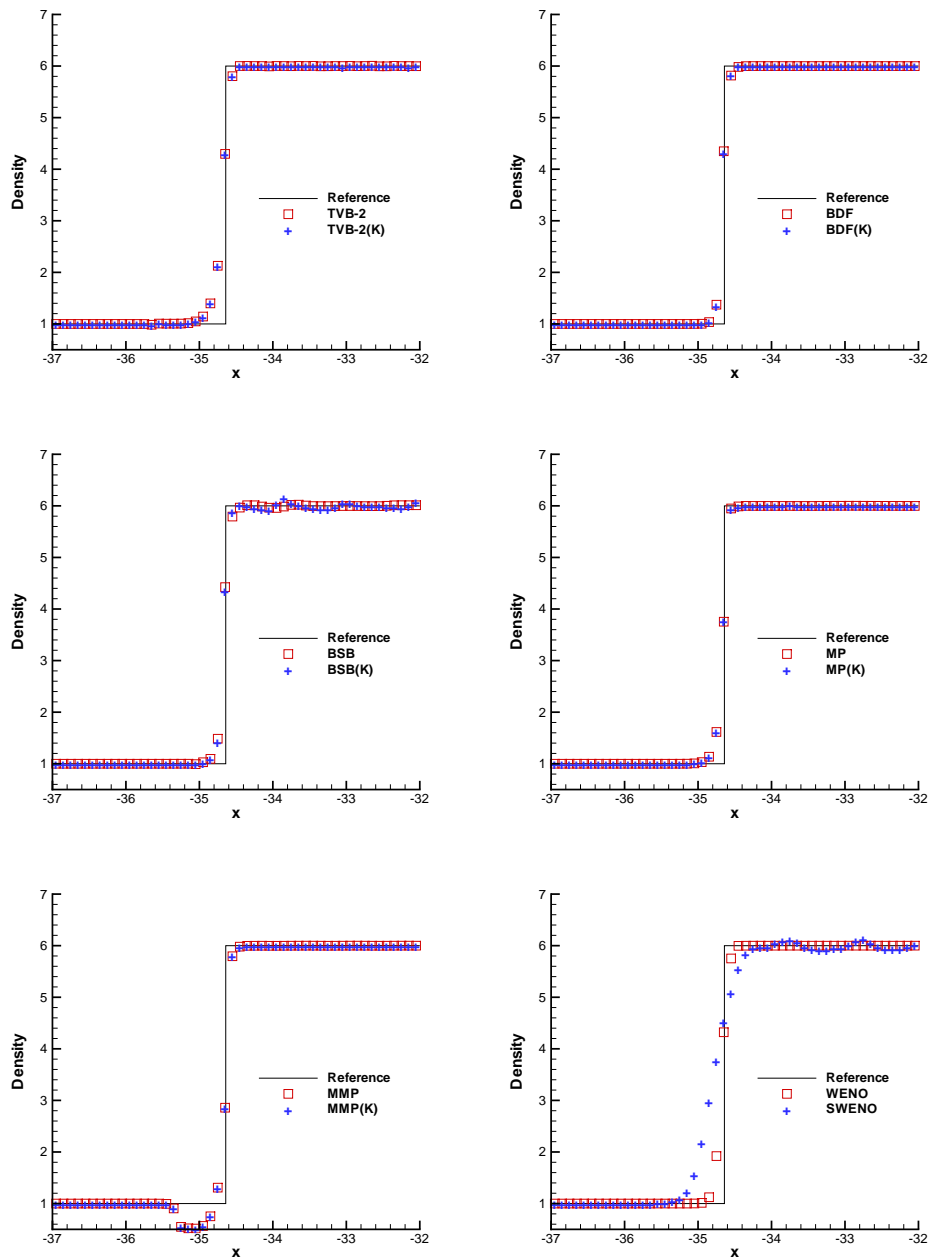
Figure 4: Single shock, density solutions, $\eta_p = 10^5$, $N = 1000$, $k = 2$.

The computational domain is $[-5,5]$ and the parameter $M = 20$ in TVB-2 limiter. We solve this problem until a simulation time of 1.3.

We plot the density solutions on $[1.4, 3.8]$ in Figs. 5 and 6. We can see from these figures that adding KXRCF shock-detector brings slight oscillations to BDF, BSB and MP
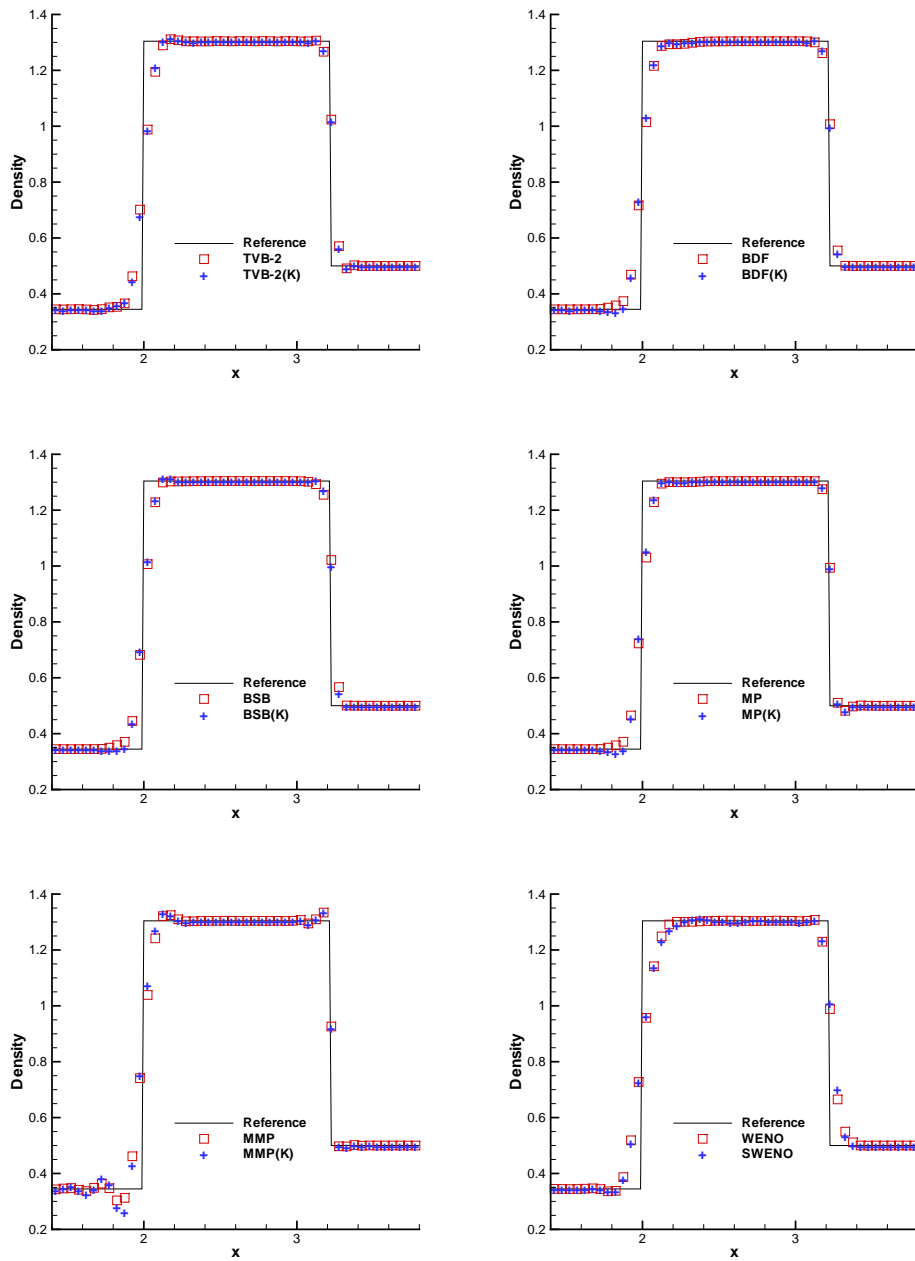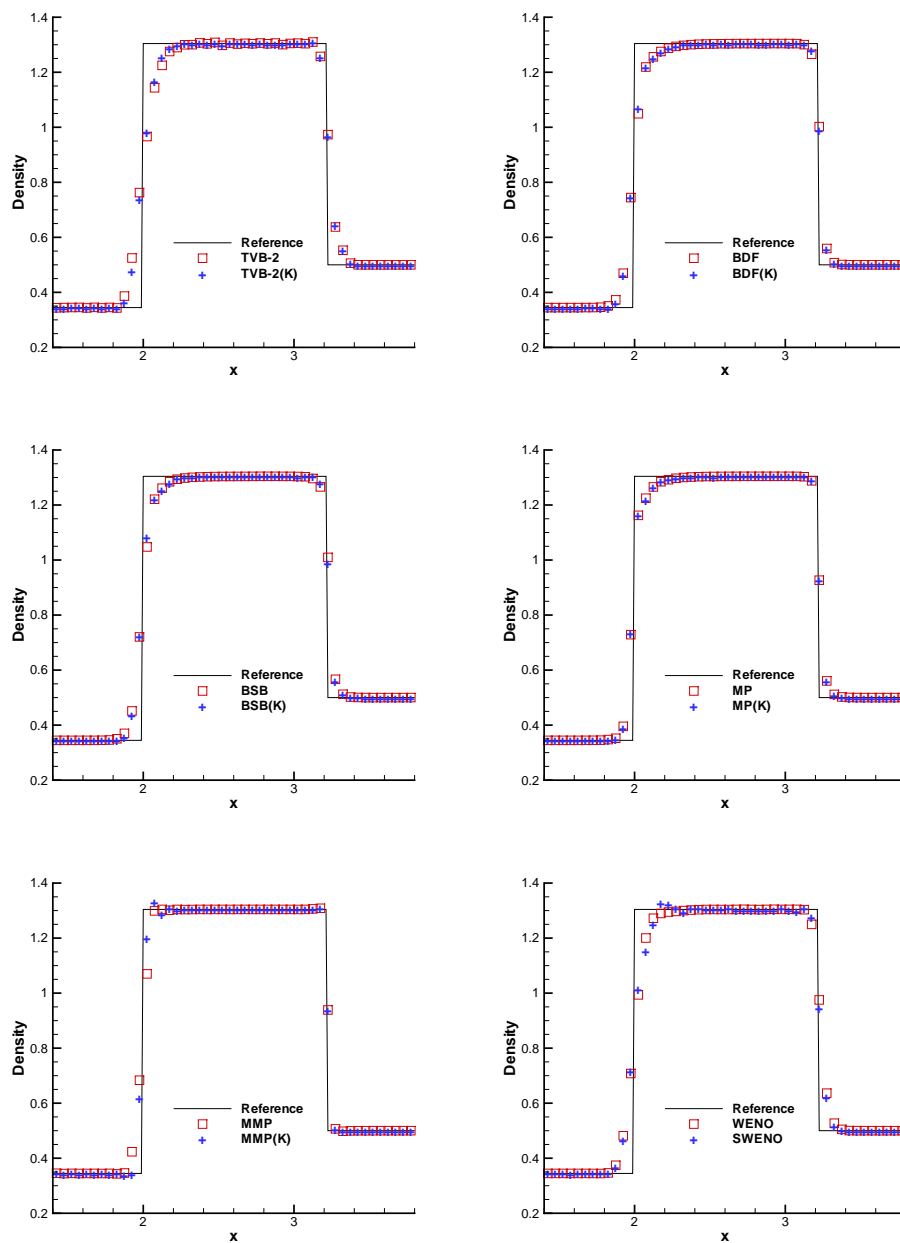
Figure 5: Lax problem, density solutions, $N=200$, $k=1$.

limiters near the contact discontinuity when $k=1$. Oscillations are also observed with MMP and MMP(K) limiters when $k=1$ and with MMP(K) and SWENO limiters when $k=2$.

We give average and maximum percentage of limited cells in Table 3. In this test

Figure 6: Lax problem, density solutions, $N = 200$, $k = 2$.

problem BDF, BSB and MP limiters again do much more limiting than the other original limiters. MMP limiter does the least limiting but it does too little to control the oscillations when $k = 1$. For KXRCF-type limiters, all of them do a considerable low amount of limiting. We also see that adding KXRCF shock-detector to the original limiters reduces the solution reconstruction work.

Table 3: Lax problem, average and maximum percentage of limited cells, $N=200$.

Limiter	$k=1$				$k=2$			
	Ave	Max	Ave(K)	Max(K)	Ave	Max	Ave(K)	Max(K)
TVB-2	1.18	2.00	0.99	2.00	1.98	4.50	1.73	4.00
BDF	24.19	40.00	2.00	3.50	36.71	64.50	2.62	5.00
BSB	32.30	58.50	1.87	3.50	35.56	62.00	2.60	5.00
MP	33.06	45.50	2.09	3.50	29.51	48.00	2.64	4.00
MMP	0.44	1.50	0.31	0.50	0.32	1.50	0.28	1.00
WENO	–	–	1.74	4.50	–	–	2.32	5.00
SWENO	–	–	2.84	6.50	–	–	2.40	5.00

Example 4.4. Shu-Osher problem [19]. Solution of this test problem contains both shocks and complex smooth regions. The initial condition is

$$(\rho,v,p) = \begin{cases} (3.857143, 2.629369, 10.333333), & \text{if } x < -4, \\ (1+0.2\sin(5x), 0, 1), & \text{if } x \geq -4. \end{cases}$$

The computational domain is $[-5,5]$ and the parameter $M=100$ in TVB-2 limiter. We solve this problem up to $T=1.8$.

Table 4 gives data of average and maximum percentage of limited cells. This table provides the same information as the previous tables. We again see that BDF, BSB and MP limiters do a lot of limiting while the others do much less. Results of density solutions on $[-3,2.5]$ are shown in Figs. 7 and 8. All the KXRCF-type limiters introduce oscillations near the small jumps when $k=1$ while all the original limiters do not. We also notice that BDF(K) and BSB(K) limiters give better approximations in the complex smooth region than BDF and BSB limiters, respectively.

Table 4: Shu-Osher problem, average and maximum percentage of limited cells, $N=400$.

Limiter	$k=1$				$k=2$			
	Ave	Max	Ave(K)	Max(K)	Ave	Max	Ave(K)	Max(K)
TVB-2	0.97	2.50	0.60	1.25	1.92	4.25	1.44	2.25
BDF	27.91	52.25	0.94	1.50	29.63	56.25	1.59	3.75
BSB	26.82	49.75	0.91	1.50	29.00	54.75	2.04	4.50
MP	22.39	39.00	1.20	1.75	22.17	37.75	1.64	3.00
MMP	0.31	0.50	0.31	0.50	0.38	0.50	0.10	0.50
WENO	–	–	1.48	2.50	–	–	1.54	3.00
SWENO	–	–	1.65	2.50	–	–	2.97	5.50
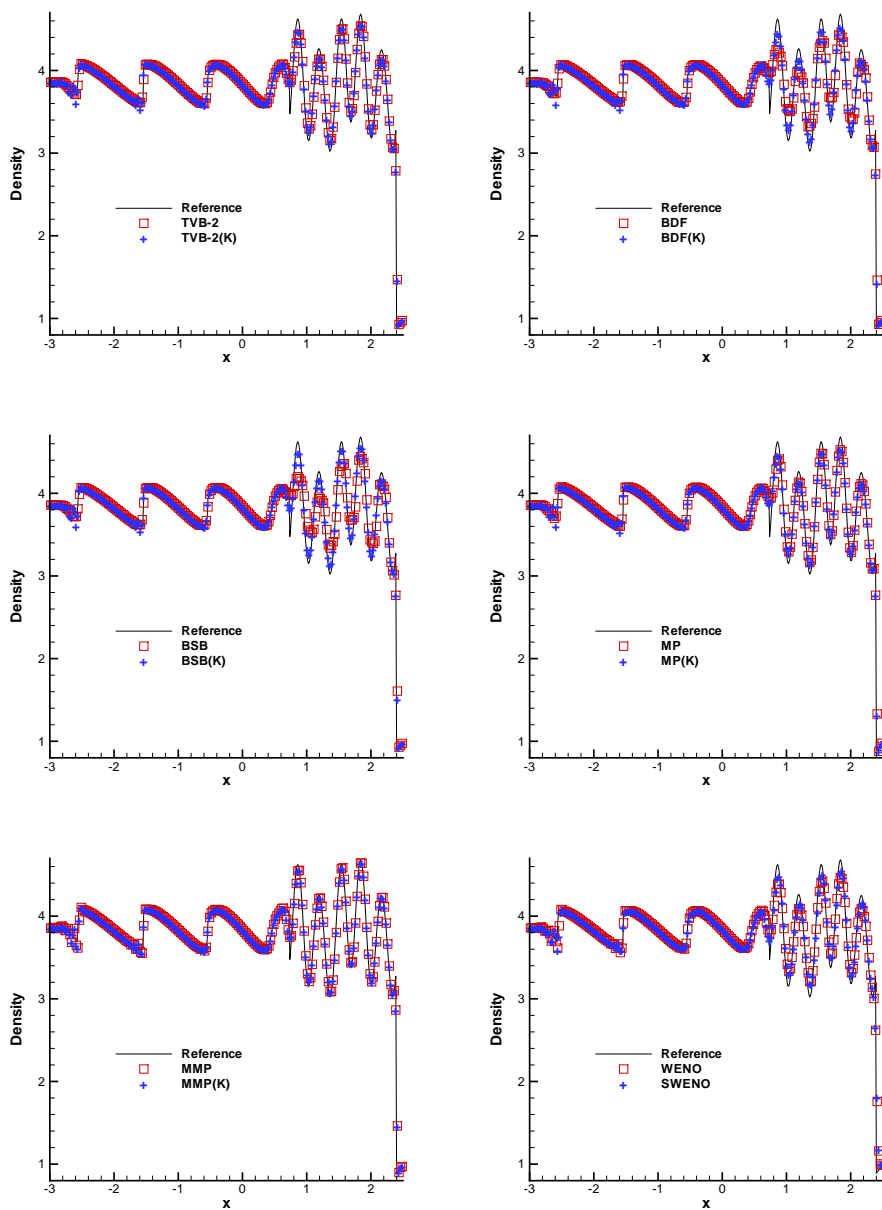
Figure 7: Shu-Osher problem, density solutions, $N = 400$, $k = 1$.

Example 4.5. The blast wave problem [23]. This classical test problem involves interaction of blast waves and its initial condition is given by

$$(\rho, v, p) = \begin{cases} (1, 0, 1000), & \text{if } 0 \leq x < 0.1, \\ (1, 0, 0.01), & \text{if } 0.1 \leq x < 0.9, \\ (1, 0, 100), & \text{if } 0.9 \leq x \leq 1. \end{cases}$$
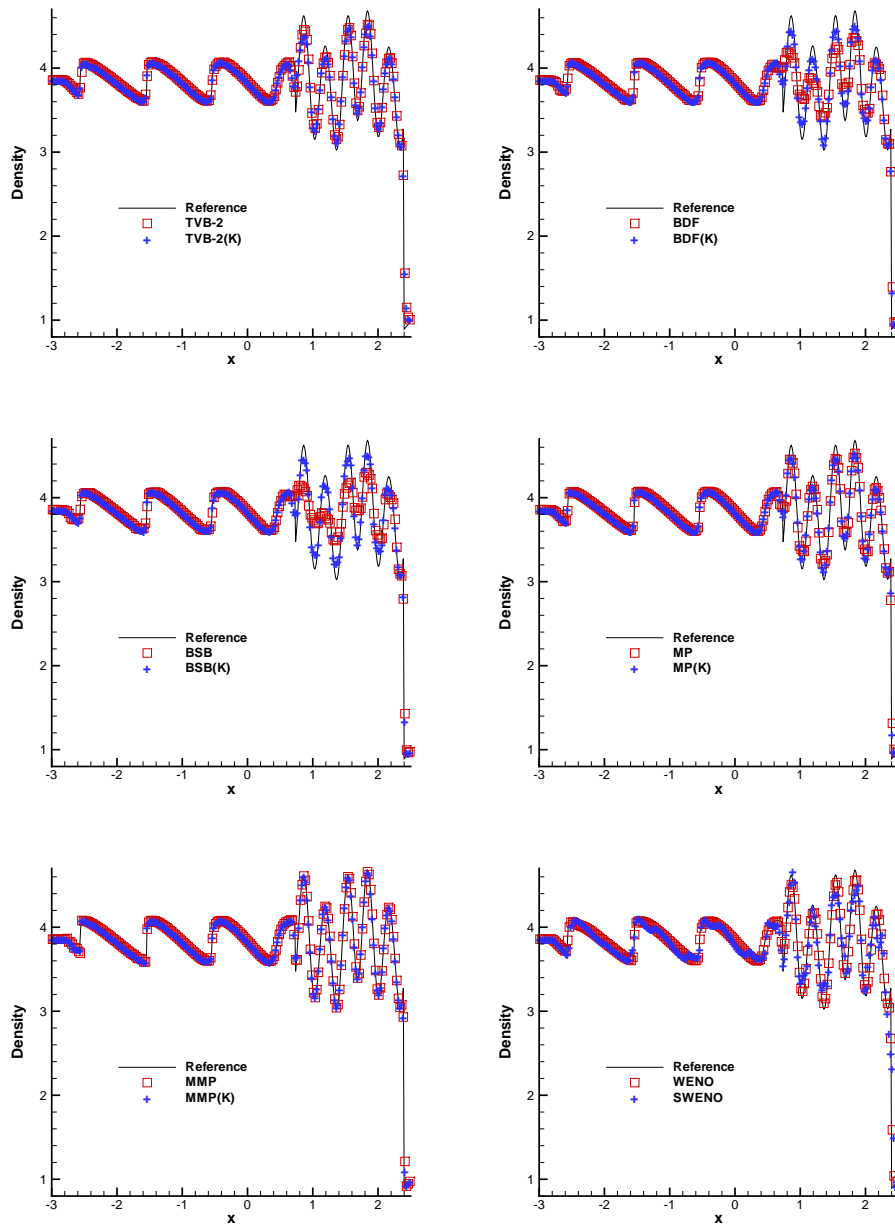
Figure 8: Shu-Osher problem, density solutions, $N=400$, $k=2$.

We compute the solution till $T=0.038$. In the TVB-2 limiter, the parameter $M=100$. Reflective boundary conditions are applied to both ends.

We give the numerical results in Table 5 and Figs. 9 and 10 (density solutions on $[0.5,0.9]$ are shown). We can see again that BDF, BSB and MP limiters result in too much limiting. MMP and MMP(K) limiters do the least limiting and give the best resolution of
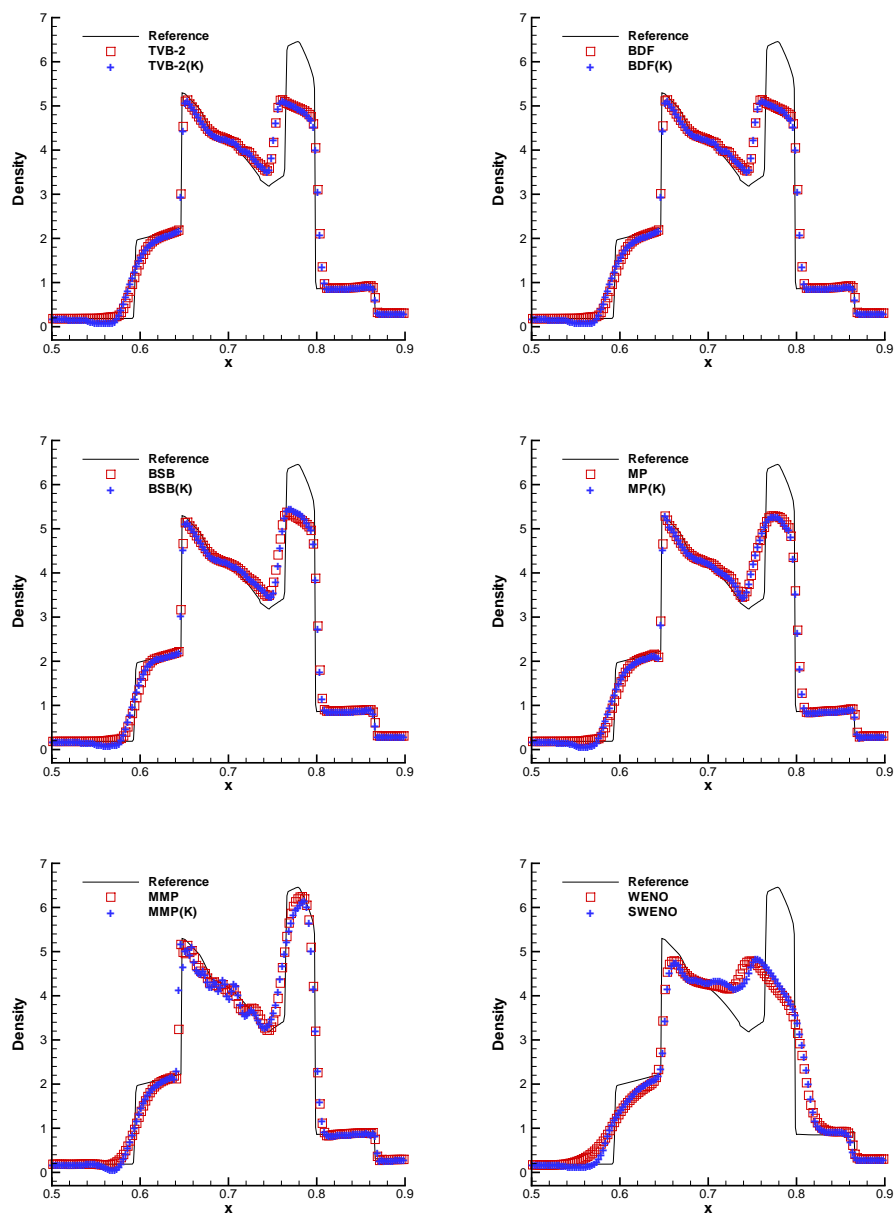
Figure 9: The blast wave problem, density solutions, $N=400$, $k=1$.

the shocks, but they introduce small oscillations. Shocks are seriously smeared and the solutions are poor with WENO and SWENO limiters.

Example 4.6. Two-dimensional Burgers equation. In this last example we consider the two-dimensional Burgers equation
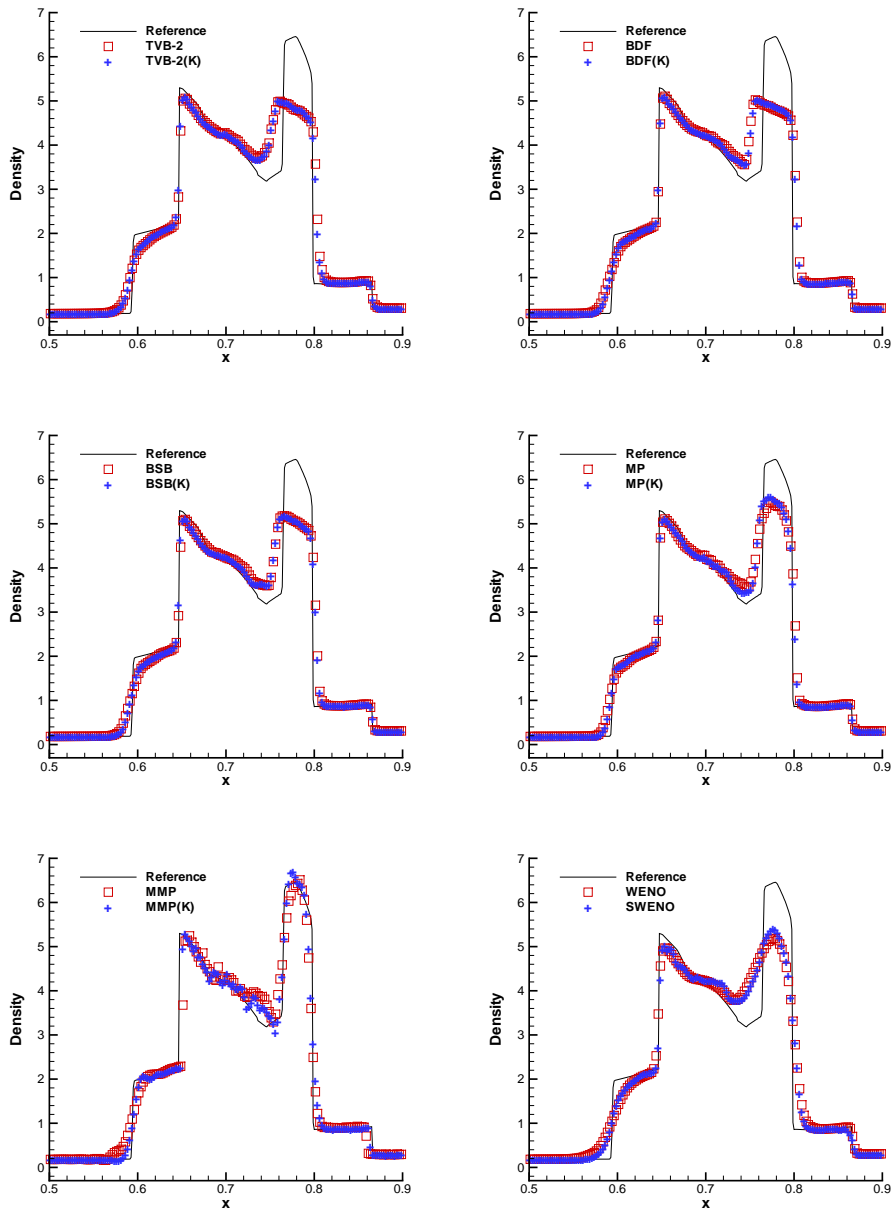
Figure 10: The blast wave problem, density solutions, $N = 400$, $k = 2$.

$$u_t + \left(\frac{u^2}{2}\right)_x + \left(\frac{u^2}{2}\right)_y = 0, \quad -2 \leq x, y \leq 2, \tag{4.2}$$

with the initial condition $u(x,y,0) = 0.5 + \sin(\pi(x+y)/2)$ and periodic boundary conditions. The exact solution is one-dimensional depending only on $\xi = x + y$; however, our

Table 5: The blast wave problem, average and maximum percentage of limited cells, $N=400$.

Limiter	$k=1$				$k=2$			
	Ave	Max	Ave(K)	Max(K)	Ave	Max	Ave(K)	Max(K)
TVB-2	4.92	7.25	4.23	7.25	10.84	15.00	8.71	13.75
BDF	47.51	74.50	6.15	9.50	54.38	85.25	11.91	19.00
BSB	48.70	78.75	5.79	10.50	56.00	91.00	11.01	18.50
MP	21.29	29.75	6.72	10.75	24.71	34.50	10.38	14.25
MMP	2.20	3.50	1.63	3.00	3.65	6.25	2.01	4.00
WENO	–	–	10.53	16.75	–	–	10.50	14.50
SWENO	–	–	13.48	20.75	–	–	16.84	24.50

Table 6: Two-dimensional Burgers equation, average and maximum percentage of limited cells, 160×80 cells.

Limiter	$k=1$				$k=2$			
	Ave	Max	Ave(K)	Max(K)	Ave	Max	Ave(K)	Max(K)
TVB-2	2.76	8.12	0.86	3.12	1.66	6.25	0.99	4.38
BDF	8.75	13.75	0.86	3.12	7.05	13.75	1.29	3.75
BSB	7.85	13.12	0.85	3.12	6.22	11.88	1.25	3.75
MP	2.16	9.38	0.90	3.12	2.13	9.38	1.44	5.62
MMP	7.04	10.62	0.62	2.50	5.32	10.00	1.03	5.00
WENO	–	–	1.15	4.38	–	–	1.48	4.38
SWENO	–	–	1.28	3.75	–	–	1.96	5.62

meshes are uniformly rectangular in the (x,y) coordinates, and thus this example is a truly two-dimensional test problem. The parameter $M=1$ in the TVB-2 limiter. We compute the solutions with 160×80 cells until $t=1.5/\pi$ and plot the solution on the diagonal cells in Figs. 11 and 12. We can see that all the limiters obtain satisfactory numerical approximations with sharp and nonoscillatory shock transitions except that overshoots are observed with MMP, MMP(K) limiters for $k=1$ and MP, MP(K), MMP, MMP(K) limiters for $k=2$. Table 6 gives data of average and maximum percentage of limited cells. We can see from this table that all the original limiters do a low amount of limiting and the amount of limiting done by KXRCF-type limiters is even lower.

5 Concluding remarks

In this paper, we numerically study and compare multiple limiters through a series of classical test problems. Detailed numerical results are presented in order to gain a better understanding of each limiter. The numerical results show that (i) TVB-2 limiter behaves consistently well in all examples but it has a parameter to tune artificially which is a serious defect of this limiter, that (ii) BDF, BSB and MP limiters usually do too much limiting, that (iii) MMP limiter often causes oscillations because it does too little limiting,
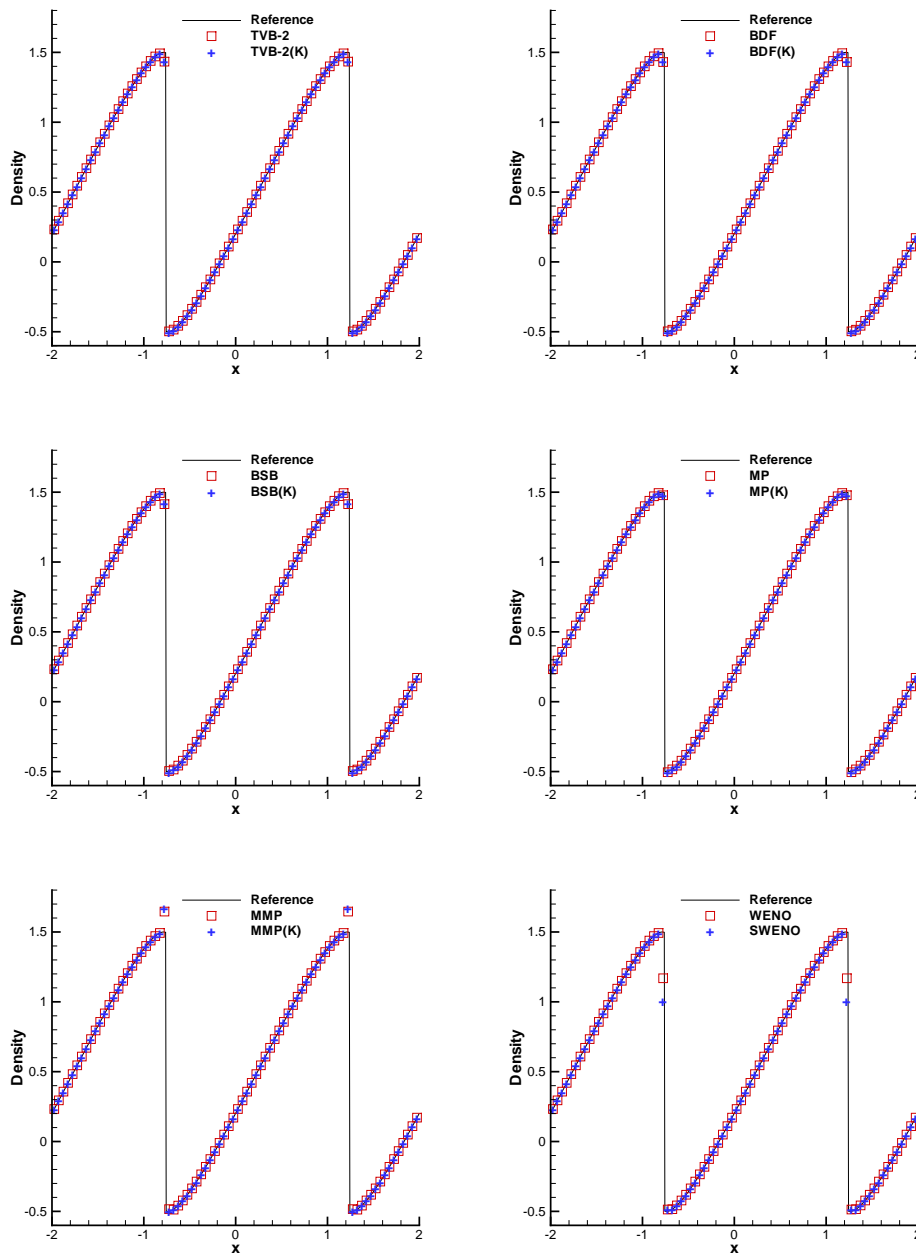
Figure 11: Two-dimensional Burgers equation, solution that cuts along the diagonal with 160×80 cells, $k=1$.

that (iv) WENO and SWENO limiters often introduce more smearing of jumps, that (v) using KXRCF shock-detector to locate discontinuities before limiting can reduce the work of solution reconstruction to a considerable low amount, but often brings oscillations when $k=1$.
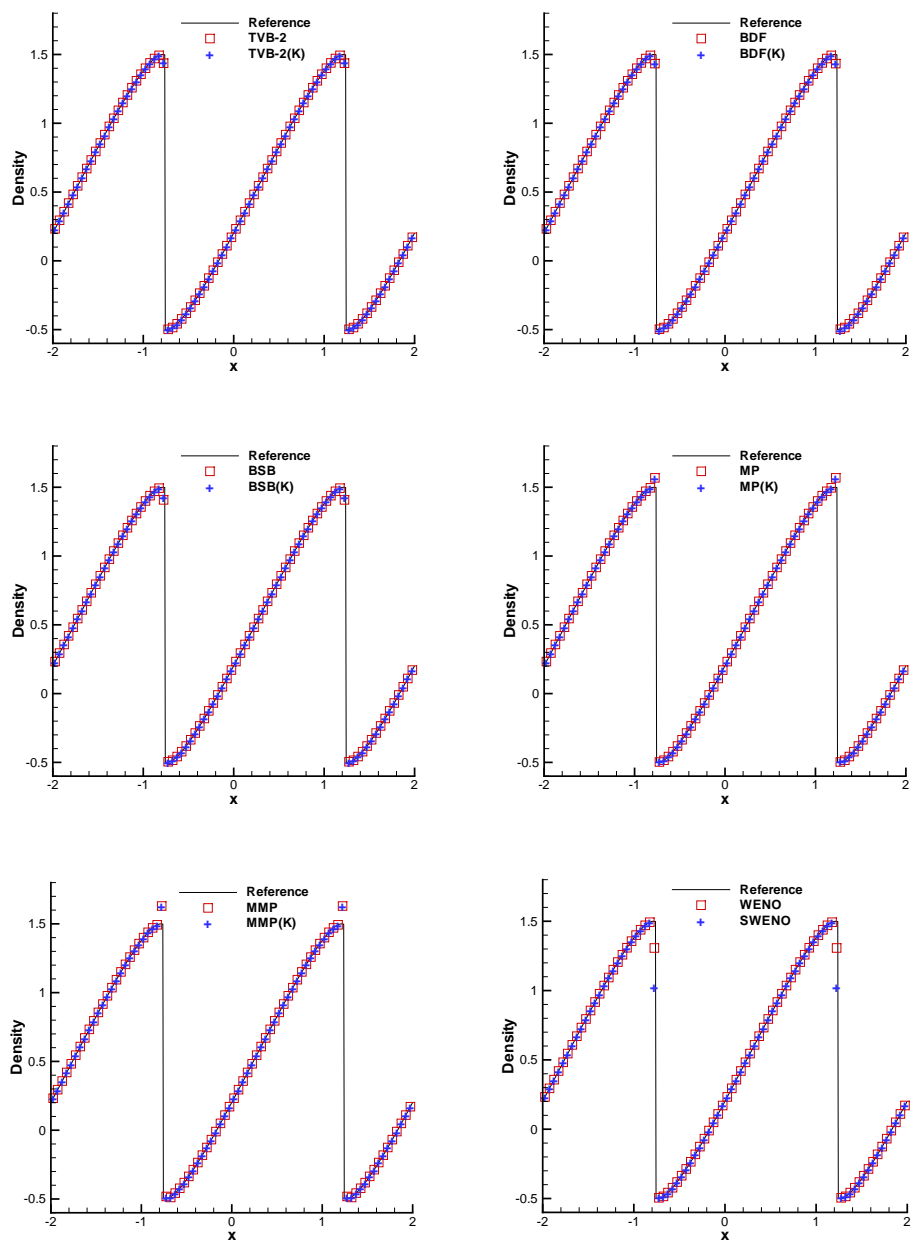
Figure 12: Two-dimensional Burgers equation, solution that cuts along the diagonal with 160×80 cells, $k=2$.

Acknowledgments

References

[1] R. BISWAS, K. DEVINE AND J. FLAHERTY, *Parallel, adaptive finite element methods for conservation laws*, Appl. Numer. Math., 14 (1994), pp. 255–283.

[2] A. BURBEAU, P. SAGAUT AND C. BRUNEAU, *A problem-independent limiter for high-order Runge-Kutta discontinuous Galerkin methods*, J. Comput. Phys., 169 (2001), pp. 111–150.

[3] B. COCKBURN, S. HOU AND C.-W. SHU, *The Runge-Kutta local projection discontinuous Galerkin finite element method for conservation laws IV: The multidimensional case*, Math. Comput., 54 (1990), pp. 545–581.

[4] B. COCKBURN, S.-Y. LIN AND C.-W. SHU, *TVB Runge-Kutta local projection discontinuous Galerkin finite element method for conservation laws III: One dimensional systems*, J. Comput. Phys., 84 (1989), pp. 90–113.

[5] B. COCKBURN AND C.-W. SHU, *TVB Runge-Kutta local projection discontinuous Galerkin finite element method for conservation laws II: General framework*, Math. Comput., 52 (1989), pp. 411–435.

[6] B. COCKBURN AND C.-W. SHU, *The Runge-Kutta local projection P^1-discontinuous Galerkin finite element method for scalar conservation laws*, Math. Model. Numer. Anal., 25 (1991), pp. 337–361.

[7] B. COCKBURN AND C.-W. SHU, *The Runge-Kutta discontinuous Galerkin method for conservation laws V: Multidimensional systems*, J. Comput. Phys., 141 (1998), pp. 199–224.

[8] B. COCKBURN AND C.-W. SHU, *Runge-Kutta discontinuous Galerkin methods for convection-dominated problems*, J. Sci. Comput., 16 (2001), pp. 173–261.

[9] G. JIANG AND C.-W. SHU, *Efficient implementation of weighted ENO schemes*, J. Comput. Phys., 126 (1996), pp. 202–228.

[10] L. KRIVODONOVA, *Limiters for high-order discontinuous Galerkin methods*, J. Comput. Phys., 226 (2007), pp. 879–896.

[11] L. KRIVODONOVA, J. XIN, J.-F. REMACLE, N. CHEVAUGEON AND J. FLAHERTY, *Shock detection and limiting with discontinuous Galerkin methods for hyperbolic conservation laws*, Appl. Numer. Math., 48 (2004), pp. 323–338.

[12] P. LAX, *Weak solutions of nonlinear hyperbolic equations and their numerical computation*, Commun. Pure Appl. Math., 7 (1954), pp. 159–193.

[13] J. QIU AND C.-W. SHU, *A comparison of troubled-cell indicators for Runge-Kutta discontinuous Galerkin mehtods using weighted essentially nonosillatory limiters*, SIAM J. Sci. Comput., 27 (2005), pp. 995–1013.

[14] J. QIU AND C.-W. SHU, *Runge-Kutta discontinuous Galerkin method using WENO limiters*, SIAM J. Sci. Comput., 26 (2005), pp. 907–929.

[15] W. REED AND T. HILL, *Triangular mesh methods for neutron transport equation*, Technical report LA-UR-73-479, Los Alamos Scientific Laboratory, Los Alamos, NM, 1973.

[16] W. RIDER AND L. MARGOLIN, *Simple modifications of monotonicity-preserving limiters*, J. Comput. Phys., 174 (2001), pp. 473–488.

[17] C.-W. SHU, *TVB uniformly high-order schemes for conservation laws*, Math. Comput., 49 (1987), pp. 105–121.

[18] C.-W. SHU AND S. OSHER, *Efficient implementation of essentially non-oscillatory shock-capturing schemes*, J. Comput. Phys., 77 (1988), pp. 439–471.

[19] C.-W. SHU AND S. OSHER, *Efficient implementation of essentially non-oscillatory shock-capturing schemes II*, J. Comput. Phys., 83 (1989), pp. 32–78.

[20] A. SURESH AND H. HUYNH, *Accurate monotonicity-preserving schemes with Runge-Kutta time*

stepping, J. Comput. Phys., 136 (1997), pp. 83–99.

[21] P. K. SWEBY, *High resolution schemes using flux limiters for hyperbolic conservation laws*, SIAM J. Numer. Anal., 21 (1984), pp. 995–1011.

[22] C. WANG, X. ZHANG, C.-W. SHU AND J. NING, *Robust high order discontinuous Galerkin schemes for two-dimensional gaseous detonations*, J. Comput. Phys., 231 (2012), pp. 653–665.

[23] P. WOODWARD AND P. COLELLA, *The numerical simulation of two-dimensional fluid flow with strong shocks*, J. Comput. Phys., 54 (1984), pp. 115–173.

[24] X. ZHONG AND C.-W. SHU, *A simple weighted essentially nonoscillatory limiter for Runge-Kutta discontinuous Galerkin methods*, J. Comput. Phys., 232 (2013), pp. 397–415.

[25] H. ZHU AND J. QIU, *Adaptive Runge-Kutta discontinuous Galerkin methods using different indicators: One-dimensional case*, J. Comput. Phys., 228 (2009), pp. 6957–6976.